Biochimie 200 (2022) 36–43

Contents lists available at ScienceDirect

Biochimie

journal homepage: www.elsevier.com/locate/biochi

# Modulation of beta-amyloid aggregation using ascorbic acid

Isabella Sampaio [a, 1], Felipe Domingues Quatroni [a, 1], Paula Maria Pincela Lins [a], Alessandro S. Nascimento [b], Valtencir Zucolotto [a, *]

[a] GNano – Nanomedicine and Nanotoxicology Group, Physics Institute of São Carlos, University of São Paulo, CP 369, 13560-970, São Carlos, SP, Brazil
[b] Molecular Biotechnology Group, Physics Institute of São Carlos, University of São Paulo, CP 369, 13560-970, São Carlos, SP, Brazil

ARTICLE INFO

*Article history:*
Received 4 March 2022
Received in revised form
18 April 2022
Accepted 11 May 2022
Available online 16 May 2022

*Keywords:*
Beta-amyloid aggregation
Ascorbic acid
Amyloid inhibitor
Alzheimer's disease

ABSTRACT

Studies have shown that the level of ascorbic acid (AA) is reduced in the brain of Alzheimer's disease (AD) patients. However, its effect on amyloid-β 1–42 ($A\beta_{42}$) aggregation has not yet been elucidated. Here we investigated for the first time the effect of AA on $A\beta_{42}$ aggregation using fluorescence assay, circular dichroism, atomic force microscopy, isothermal titration calorimetry, ligand docking, and molecular dynamics. Our results showed that the fibril content decreases in the growth phase when the peptides are co-incubated with AA. AA molecules bind to $A\beta_{42}$ peptides with high binding affinity and a binding site for AA between the β-strands of $A\beta_{42}$ oligomers prevents the stack of adjacent strands. We demonstrate the inhibitory effect of AA on the aggregation of $A\beta_{42}$ and its molecular interactions, which can contribute to the development of an accessible therapy for AD and also to the design of novel drugs for other amyloidogenic diseases.



## 1. Introduction

Alzheimer's disease (AD) is characterized by memory impairment and cognitive decline [1], predominantly affecting elderly people. The accumulation of amyloid-β (Aβ) plaques around neurons has been indicated as a key process in AD pathogenesis [2]. Aβ peptides are generated at different lengths through cleavage of the amyloid precursor protein by the beta-secretase 1 (BACE1) enzyme, with the 42-amino acid peptide ($A\beta_{42}$) being the most neurotoxic one [3,4]. $A\beta_{42}$ has a hydrophobic C-terminal region that undergoes conformational changes, forming a β-sheet secondary structure with a high aggregation tendency [5–7]. The self-assembly of these peptides generates fibrils and amyloid plaques, which exert neurotoxic effects such as oxidative stress, inflammation, and synaptic loss [8–10]. Currently, AD is treated with drugs that only mitigate the symptoms. Alternative therapeutic strategies that target $A\beta_{42}$ have been investigated, including BACE1 inhibitors and immunotherapies aimed at stimulating the immunological response to Aβ or to avoid amyloid aggregation by binding monoclonal antibodies to the peptides [4,9]. However, these strategies have not shown significant clinical benefits, and many of them present side effects [11,12]. Novel inhibitors of amyloid aggregation are desirable for developing an effective treatment for AD.

Ascorbic acid (AA) is an essential antioxidant molecule and a human dietary component involved in many physiological processes, including generation of immunological responses and maintenance of endothelial integrity [13–15]. The highest concentration of AA (1–2 mM) [16] is found in the cerebrospinal fluid, and the sodium-dependent vitamin C transporter-2 (SVCT2) is responsible for mediating its transport into the brain and neurons [16–18]. AA is required as a cofactor for neurotransmitter synthesis, promotes synaptic maturation, and is responsible for scavenging free radicals, protecting neuronal cells from oxidative damage [13,15]. Low levels of AA in the brain are associated with an increase in the amount of amyloid plaques and cognitive impairment [19–21]. Kook et al. showed that AA supplementation in an AD mouse model has a neuroprotective effect, reducing amyloid plaque formation and reactive oxygen species generation [22]. Noguchi-Shinohara et al. reported that among elderly women harboring the apolipoprotein E gene (APOE E4), a risk factor for AD, they observed a lower incidence of cognitive decline in individuals with higher levels of blood AA [23]. In addition, an inhibitory effect of AA was observed on amyloid fibrillation of human insulin [13,18] and hen egg-white lysozyme [24]. These studies indicate that AA plays an important role in protecting the brain against

* Corresponding author.
*E-mail address:* zuco@ifsc.usp.br (V. Zucolotto).
[1] Authors with equal contributions.

https://doi.org/10.1016/j.biochi.2022.05.006
0300-9084/

neurodegeneration caused by amyloid-related diseases.

To the best of our knowledge, no studies have explained the modulation of $A\beta_{42}$ aggregation by AA. Here, we investigated the effect of AA on $A\beta_{42}$ aggregation to evaluate its therapeutic potential against AD. The molecular interactions involved in the aggregation kinetics were also studied to elucidate the mechanism of action of AA.

## 2. Materials and methods

### 2.1. Materials

β-amyloid (1-42) peptide fragment (cat. no. A9810), dibasic sodium phosphate (cat. no. S5136), monobasic sodium phosphate dihydrate (cat. no. 71500), L-AA (cat. no. A5960), thioflavin T (cat. no. T3516), sodium chloride (NaCl, cat. no. S7653), and sodium hydroxide (NaOH, cat. no. S8045) were purchased from Sigma-Aldrich.

### 2.2. Study design

The formation of $A\beta_{42}$ aggregates was evaluated using fluorescence techniques with the marker thioflavin T (ThT), atomic force microscopy (AFM), and circular dichroism (CD), while the type of interaction between AA molecules and $A\beta_{42}$ monomers was studied using isothermal titration calorimetry (ITC), ligand docking, and molecular dynamics (MD). This study was not pre-registered and institutional ethical approval was not required. No randomization and blinding tests were performed, and no inclusion or exclusion criteria were applied. The sample size was based on previous studies.

### 2.3. Preparation and incubation of Aβ42

The lyophilized $A\beta_{42}$ was solubilized in 1 mM NaOH, filtered through a 0.2 μm Millipore filter, and then diluted in phosphate buffered saline (PBS) (10 mM, 0.1 M NaCl, pH ~7.4). To determine the $A\beta_{42}$ concentration, the absorption at 280 nm was measured in a Nanodrop One (Thermo Fischer Scientific) using a molar extinction coefficient of 1490 $M^{-1}$. $cm^{-1}$. Samples of $A\beta_{42}$ 10 μM were prepared with and without AA 250 μM in PBS buffer for ThT fluorescence and AFM experiments. For CD analysis, aliquots of 30 μM $A\beta_{42}$ were prepared with or without AA (250 μM) in PBS buffer. All samples were prepared in triplicate and incubated in a MS-100 thermoshaker incubator for 72 h at 37 °C and 300 rpm.

### 2.4. ThT fluorescence assay

The formation of amyloid fibrils was evaluated using a ThT fluorescence test. The ThT stock solution was freshly prepared in methanol, filtered through a 0.2 μm Millipore filter, and diluted in deionized water. At 24 h intervals, aliquots of incubated samples were collected to prepare solutions containing $A\beta_{42}$ 2 μM and ThT (4 μM), which were added to a 96-well plate. The fluorescence of the solutions was measured in the top read mode using a SpectraMax Microplate Multi-mode M3 Reader (excitation at 440 nm, emission at 480 nm). A control sample containing only AA in PBS and incubated under the same conditions was also analyzed and used to normalize the fluorescence intensity of the samples with $A\beta_{42}$ + AA. For the samples without AA, ThT fluorescence only in PBS was used for normalization. All tests were performed in triplicate.

### 2.5. Statistical analyses

Statistical analyses of fluorescence data were performed using Microsoft Excel (Microsoft 365) by applying one-way and two-way analysis of variance (ANOVA) models. One-way ANOVA was performed to determine the statistical difference among all incubation times for the same group. Two-way ANOVA with repetition was performed to compare differences between groups 1 and 2 at different incubation times. For all comparisons, an alpha of 0.05 was used; $p < 0.05$ was considered significant.

### 2.6. AFM

At 24 h intervals, 10 μL of the incubated sample was collected and dripped onto mica. After 10 min, the mica was carefully washed with deionized water to remove excess salt from the buffer and dried in a desiccator for 12 h. AFM images were obtained using a NanoSurf Flex AFM microscope Flex-Axiom with a TAP300AL-G tip and processed using the Gwyddion software. The average height of the fibrils was determined from the cross-sectional contours of 3 fibrils ($n = 3$) in the AFM images of each sample.

### 2.7. ITC

ITC measurements were performed in a Malvern Microcal ITC200 at 37 °C with 50 μM $A\beta_{42}$ monomers in the sample cell and AA 5 mM in the syringe, both in the same buffer (10 mM PBS, 192 μM NaOH, pH 7.4). Initially, 0.4 μL of AA was titrated, followed by 35 additional injections of 2 μL of AA, at intervals of 180 s, until a saturation profile was observed in the isotherm. The isotherm was obtained using Origin 7.0 provided by MicroCal ITC and its fitting was performed using the NanoAnalyse 3.1 software, which determined the interaction model and thermodynamic values. To obtain the heat of dilution, AA 5 mM in the injector was titrated into the buffer in the sample cell under the same conditions as the interaction experiment. The experiments were performed in triplicate.

### 2.8. CD

The CD measurements were performed on a Jasco J-715 spectropolarimeter in a 0.1 cm optical path cuvette and in the range of 200–280 nm. Samples of $A\beta_{42}$ (30 μM) with and without AA (250 μM) were incubated for 72 h and analyzed every 24 h, as were the controls of PBS (10 mM) and AA (250 μM). The data were processed in CDToolX, and each spectrum was generated through an average of six scans as a function of ellipticity (mdeg). The β-sheet content was determined using K2D3 software as a function of molar extinction (Δε).

### 2.9. Ligand docking and simulation

The first attempt to identify a binding pocket in the $A\beta_{42}$ fibrils (PDB ID 2BEG [25]) did not reveal a reasonable pocket for AA. Considering the molecular stoichiometry observed in the ITC data, we generated a pre-fibrillar structure by removing the central strand in the $A\beta_{42}$ NMR structure to generate two units with two β-strands in each unit. A search for a cavity in this structure revealed a suitable pocket that was used for docking calculations with LiBELa [26]. The (5-stranded) $A\beta_{42}$ NMR structure, the pre-fibrillar structure, and the pre-fibrillar structure bound to AA were used in MD simulations using the AMBERFF19SB force field and the AMBER package [27–29]. The data obtained from a productive 300-ns NPT simulation TIP3P solvent for each system were used for analysis, using CPPTRAJ [30], AmberEnergy++ [31]. Each system was neutralized, and Na+ and Cl-ions were added to ensure a final concentration of 150 mM NaCl in the simulation box. Figures were prepared using the VMD [32] and UCSF Chimera [33].

### 2.10. Protein Data Bank (PDB) — acession numbers

The acession ID of the $A\beta_{42}$ fibrils structure used in the molecular dynamics is PDB ID 2BEG.

## 3. Results

### 3.1. Inhibition of $A\beta_{42}$ fibrillation by AA molecules

Samples containing $A\beta_{42}$ monomers (10 μM) and AA (250 μM) (Group 2) were incubated under pro-aggregation conditions (37 °C, 300 rpm) for 72 h. As controls, samples containing only $A\beta_{42}$ monomers (10 μM) (Group 1) were incubated under the same conditions (Fig. 1A).

To monitor amyloid aggregation, aliquots of the $A\beta_{42}$ monomer samples with or without AA were collected at 24 h intervals and analyzed using AFM and Thioflavin T fluorescence assays. For each test, three independent aliquots were analyzed (n = 3). Sample sizes were chosen based on previous studies [34,35]. ThT is a fluorescent probe whose emission increases upon binding to β-sheet structures and has been extensively used to quantify amyloid fibrils [36–38]. In this study, a fluorescence assay was employed to compare the formation of fibrils between groups 1 and 2. As shown in Fig. 1B, for samples without AA, the intensity of ThT fluorescence increased over time, with an increase of 57% between 24 h and 72 h, demonstrating that the $A\beta_{42}$ aggregated into β-sheet-rich fibrils. When the $A\beta_{42}$ samples were incubated with AA, a significantly lower fluorescence intensity was observed for all incubation times. Interestingly, for this group, the ThT emission decreased by 39% in the 24–72 h interval. After 72 h of $A\beta_{42}$ incubation under pro-aggregation conditions, the mean fluorescence value was 77% lower in samples containing AA than in those without AA. These results reveal that AA has a significant effect on amyloid aggregation by inhibiting fibrillation. Although sample preparation was performed to contain only monomers, the ThT signal after 72 h for samples with AA is lower than at t = 0, which may indicate that there were some aggregates in the samples at the beginning of incubation. The AFM images (Fig. 2A) corroborated the fluorescence analysis results; although fibril formation was observed in both samples (Groups 1 and 2) after 24 h of incubation, fibrillar aggregates were found in the growth phase (24–72 h) only in the samples without AA. The height distribution of the fibrils was determined from the cross-sectional contours of the AFM images (Fig. 2B). In the 24–72 h interval, the height of the fibrils increased from 8.1 ± 1.6 to 31.0 ± 1.8 nm in the absence of AA, while the height decreased from 12.1 ± 0.5 to 6.8 ± 0.6 nm for peptides co-incubated with AA. A decrease in fibril height was also reported in previous studies using other inhibitors [34,35]. Fluorescence and AFM data indicated that AA could reverse fibrillation during the initial stage of aggregation.

CD analysis was performed to assess transitions in the secondary structure during amyloid aggregation. Samples containing 30 μM $A\beta_{42}$ were incubated in the absence or presence of AA (250 μM). Fig. 3 shows the CD spectra, in which the characteristic band of β-sheet structures (at 220 nm) was observed after 24 h of incubation for both samples, confirming the transition of unstructured native monomers to β-sheet-rich structures. In contrast to the ThT and AFM results, the samples of the two groups presented similar CD spectra. As discussed by Jiang et al. [39], the ThT probe identifies orderly stacked β-sheets, which are found in fibrillar aggregates. Therefore, co-incubation with AA may not have a remarkable effect on the conformational changes of $A\beta_{42}$ peptides but may inhibit fibrillar aggregation. Notably, the ratio of $A\beta_{42}$ to AA concentrations was lower in the CD assay, suggesting that AA has a dose-dependent effect on $A\beta_{42}$ aggregation. Earlier reports also showed a dose-dependent effect of AA on the inhibition of insulin fibrils [18]. Despite the similar spectra, the evolution of β-sheet content as a function of incubation time (Table 1) was different between the groups. After 24 h, the β-sheet content increased with time for $A\beta_{42}$ incubated without AA, but decreased for AA-containing samples. In addition, although the fluorescence tests indicate the presence of pre-aggregated structures at the beginning of the incubation, the CD spectra are typical of the monomeric form of the peptide. Thus, we can conclude that the samples contained both monomers and small oligomers (for example, dimers and tetramers) that cannot be distinguished from each other by this technique.

### 3.2. High binding affinity between AA and $A\beta_{42}$ monomers

ITC was used to model the inhibitory effect of AA on the formation of amyloid fibrils. The AA dilution heat was evaluated (Fig. S1, Supporting Information) and showed a minimal and sequential heat of dilution (0.085 ± 0.005 μcal/s) that did not affect the interaction measurements. Then, AA 5 mM was titrated to 50 μM $A\beta_{42}$ monomers in the same buffer (10 mM PBS, 192 μM

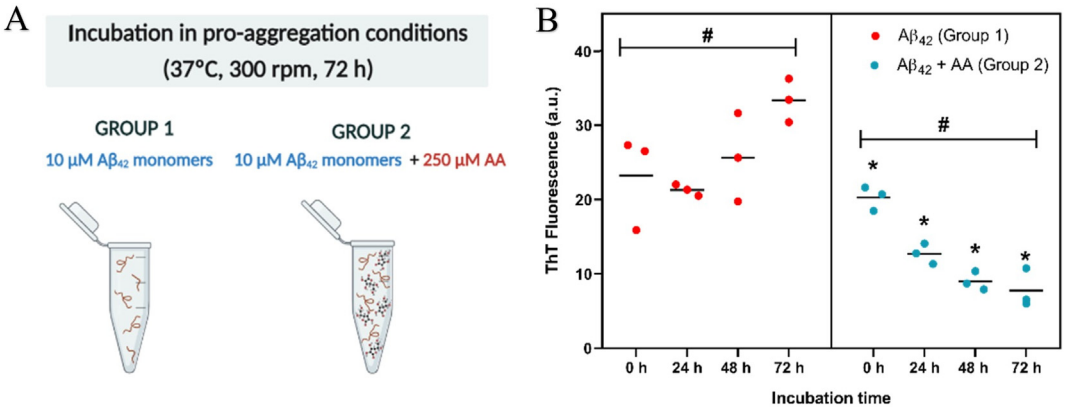


**Fig. 1.** — **(A)** Schematic view of the groups used to evaluate the AA effect in $A\beta_{42}$ aggregation. Created with biorender.com. **(B)** ThT fluorescence intensity of samples containing 10 μM $A\beta_{42}$ monomers at 480 nm wavelength after incubation at 37 °C for 0, 24, 48 or 72 h in the absence (red points) or presence of AA (250 μM; blue points). The fluorescence intensity of ThT and ThT + AA was used in the data normalization. The measurements and errors are represented by average and standard deviation, respectively. *Statistically different ($F_{(1.16)} = 106.27$, $p < 0.001$) from group 1 at the same incubation time; #Statistically different between all incubation times of the same group ($F_{(3.8)} = 6.81$, $p < 0.02$ for group 1 and $F_{(3.8)} = 29.67$, $p < 0.01$ for group 2); all tests were performed with n = 3, where n is the number of independent aliquots, an $\alpha = 0.05$.

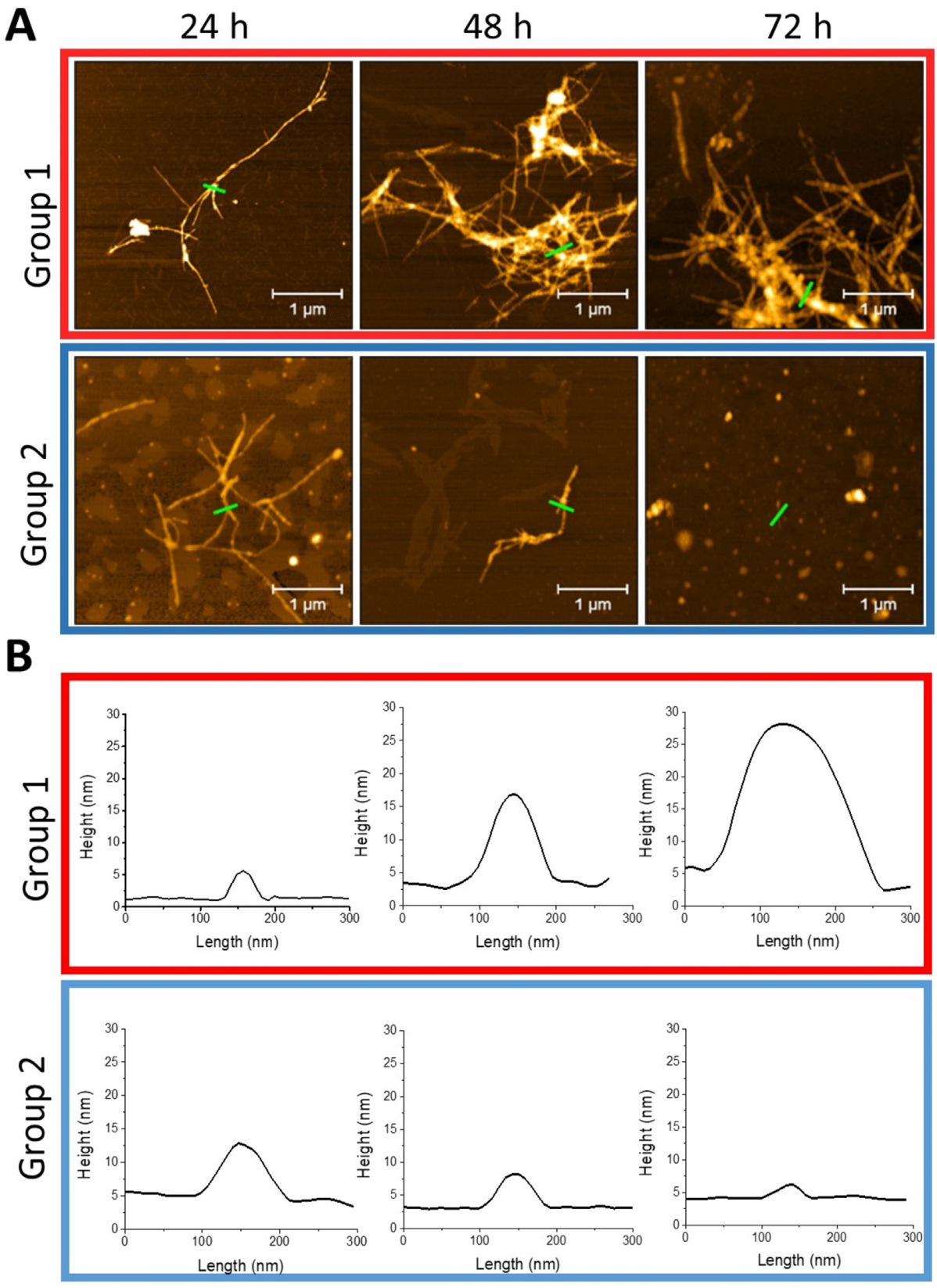


**Fig. 2.** – **(A)** AFM images of $A\beta_{42}$ 10 µM incubated at 37 °C for 24, 48 or 72 h with or without AA. Scale: 4 µm × 4 µm. Green bars represent the cross-sectional contour used to determine fibril height. **(B)** Fibrils height determined from AFM images of $A\beta_{42}$ incubated in pro-aggregation conditions with or without AA for 24, 48, and 72 h.

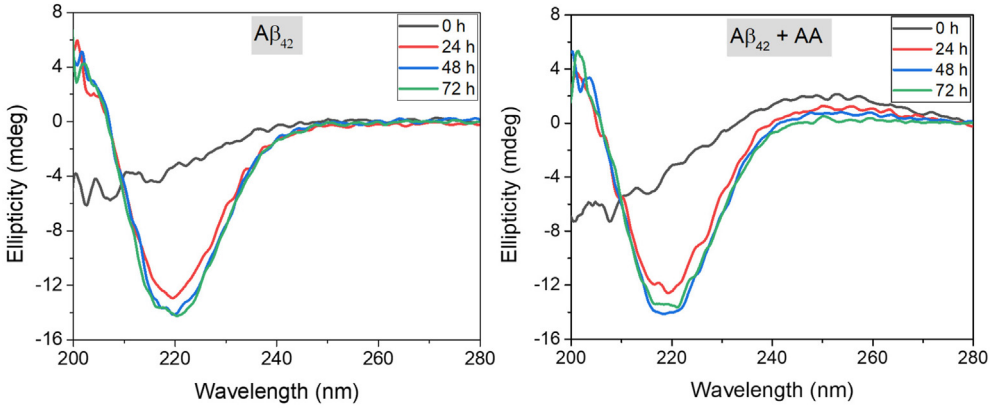


**Fig. 3.** Secondary structure study of $A\beta_{42}$. Circular dichroism spectra over time of $A\beta_{42}$ 30 μM incubated at 37 °C in the absence (left) and presence of AA 250 μM (right).

**Table 1**
- Beta-sheet content of the samples over time determined from CD measurements using K2D3 software.

| Incubation time | β-sheet content | |
|---|---|---|
| | $A\beta_{42}$ | $A\beta_{42}$ + AA |
| 0 h | 17.9% | 15.7% |
| 24 h | 32.6% | 35.1% |
| 48 h | 33.1% | 34.4% |
| 72 h | 33.7% | 34.1% |

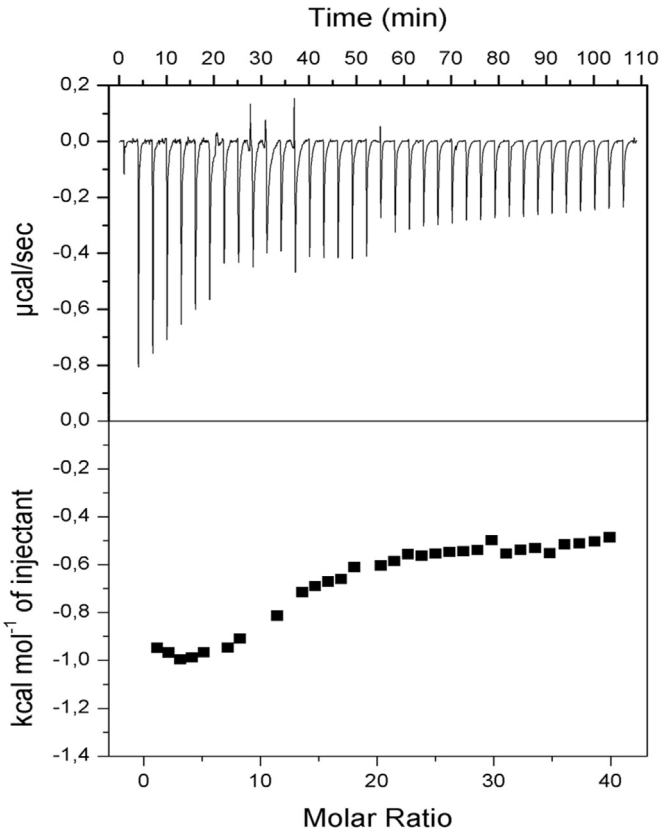


**Fig. 4.** ITC isotherm revealing the interaction between AA and $A\beta_{42}$ monomers. AA (5 mM in the syringe) was titrated to 50 μM $A\beta_{42}$ monomers in the sample cell. The experiment was performed in 10 mM PBS and 192 μM NaOH at pH 7.4 and 37 °C.

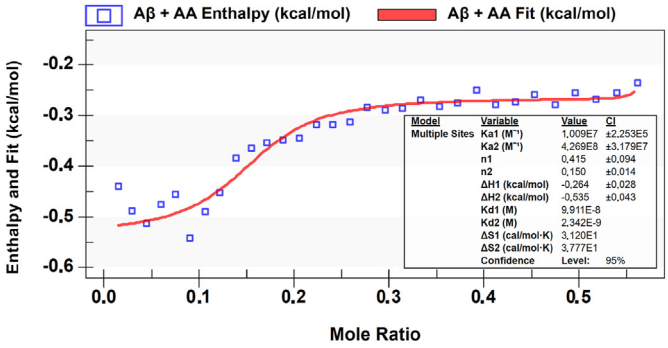


**Fig. 5.** Fitting curve and thermodynamic parameters of the binding between $A\beta_{42}$ monomers and AA. The parameter values were determined by the NanoAnalyse 3.1 software using the multiple binding sites model and a 95% confidence interval (CI).

NaOH, pH 7.4), with a 100-fold higher concentration of the ligand than of the substrate. The isotherm in Fig. 4 shows the binding of AA molecules to the monomers through an exothermic reaction (negative peaks) and the typical shape of a receptor containing two binding sites with different affinities [40,41].

The fitting of ITC data was performed using the NanoAnalyse 3.1, which also provided the thermodynamic parameters. Four points were excluded from the ITC curve, since the noise from these points did not enable a precise integration for the post-analysis. This may have resulted, for example, from a bubble in the system for these injections. This is a common procedure in the software of the analysis used. The model that best fitted the curves was cooperative binding with multiple sites (Fig. 5). Based on the association ($K_a$) and dissociation constants ($K_D$), we determined that the interaction occurred through positive cooperative binding with two sites. In this interaction mode, the binding affinity of the AA molecules increased as the peptide binding sites were occupied ($K_{a2} > K_{a1}$). The binding of AA to $A\beta_{42}$ has a non-integer stoichiometry, which may suggest the binding to the small oligomers instead of AA binding to monomers, where a 1:1 stoichiometry would be observed. Other molecules such as Tabersonine [35] and Ginnalin A [34] have also been reported to inhibit fibrillar aggregation upon binding to monomers or oligomers. However, AA exhibits low $K_D$ values ($K_{D1} = 99.11 \times 10^{-9}$; $K_{D2} = 2.34 \times 10^{-9}$, as shown in Table 2), indicating a high binding affinity to $A\beta_{42}$ peptides. In addition, many studies have indicated that natural compounds with anti-oxidant properties are promising molecules for AD treatment. For

**Table 2**
Comparison of $K_D$ values of inhibitors of $A\beta_{42}$ fibrillation.

| Inhibitors of $A\beta_{42}$ fibrillation | $K_D$ (nM) | Ref |
|---|---|---|
| Aβ-Apt | 63.4 | [45] |
| AA | 99.1 | This work |
| Ginnalin A | 3500 | [34] |
| Tabersonine | 6900 | [35] |

example, curcumin derivatives have been extensively explored [42–44]; however, their rapid metabolism and low absorption are challenges that need to be overcome in order to deliver therapeutic concentrations to the brain. In this sense, the use of AA is also advantageous as it tends to accumulate in the brain [15,16].

### 3.3. AA binding prevents β-sheet stacking of $A\beta_{42}$ oligomers

The atomic details of the interaction between AA and $A\beta_{42}$ were also evaluated using ligand docking and MD simulations. Based on our previous results that indicated AA binding to small oligomers, we chose the NMR structure of pentamers (PDB ID 2BEG [25]), which has been reported to be the most predominant aggregated form during the lag phase and also act as seeds in amyloid aggregation [6,34]. The first attempt to identify a binding pocket in the $A\beta_{42}$ pentamers did not reveal a reasonable pocket for AA (Fig. S2, Supporting Information). Considering the molecular stoichiometry observed in the ITC data, we generated a pre-fibrillar structure by removing the central strand in the $A\beta_{42}$ NMR structure to generate two units with two β-strands in each unit. The low-energy docking pose suggested favorable polar interactions between AA and Asp23 and Lys28 of adjacent strands, showing a reasonable pocket for AA using this structure (Fig. 6A).

MD simulations of the $A\beta_{42}$ pentamer (Fig. 6B) indicated that the interaction between Asp23 and Lys28 accounted for at least 60% of the total interstrand interaction energy. This finding suggests that AA competes with other $A\beta_{42}$ monomers to bind to the β-strand surface of oligomers. When the central β-strand was removed (Fig. 6C), we rapidly observed the formation of a tetramer,

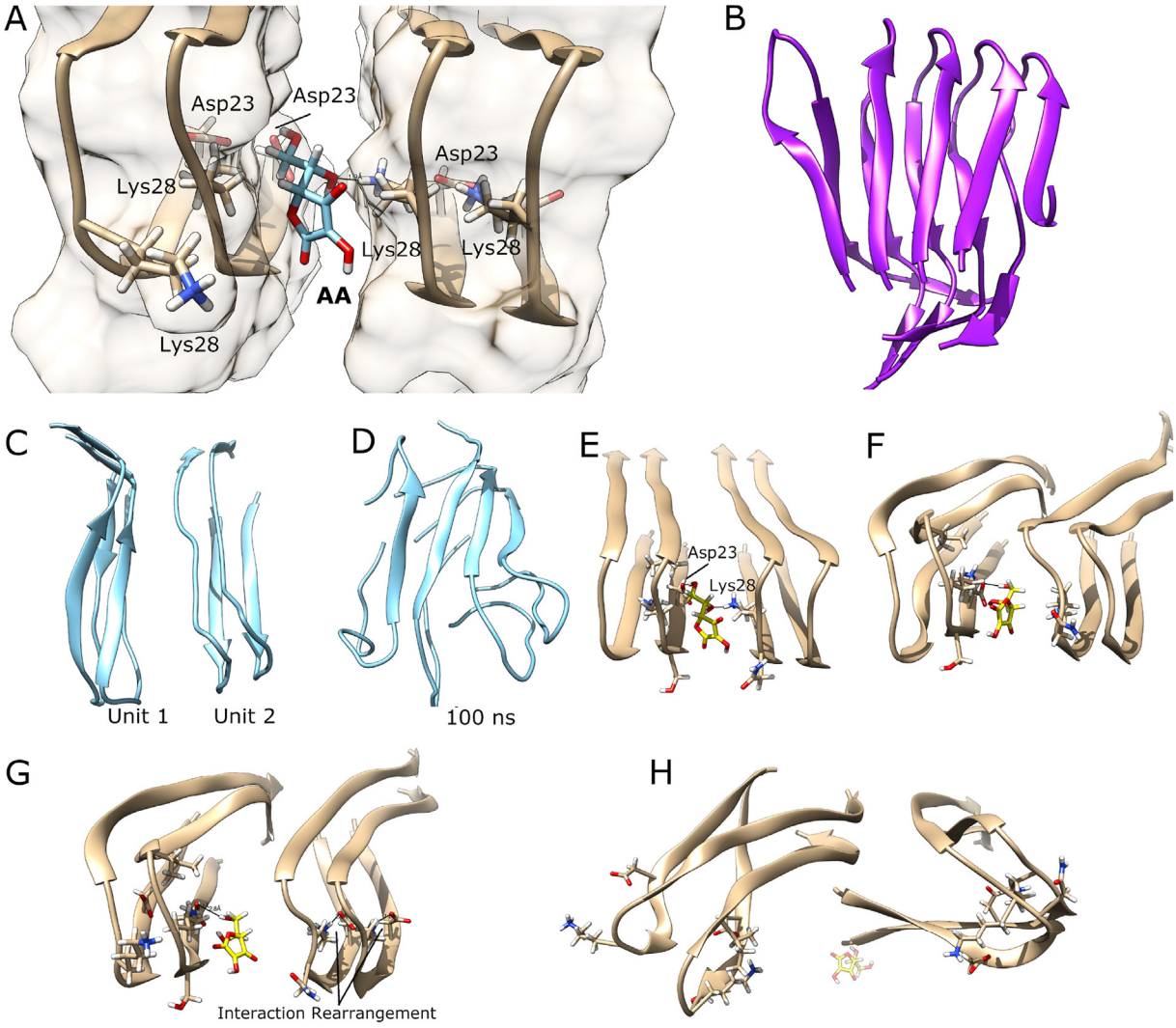


**Fig. 6.** Ligand docking and MD studies of the binding interactions between $A\beta_{42}$ and AA. (A) Docking of AA in a cleft between β-strands 2 and 4 in the $A\beta_{42}$ fibrils. The ligand interacts with Asp23 (β-strand 2) and Lys 28 (β-strand 4). (B) $A\beta_{42}$ fibrils (PDB ID 2BEG) after 300 ns of MD simulation. The structure of the fibrils is very stable over time. (C) $A\beta_{42}$ pre-fibrillar structure and (D) conformation obtained after 100 ns of MD simulation. Here, a four-stranded structure was obtained in an equilibrium simulation. (E to H) Time evolution of the MD simulation of the AA-bound $A\beta_{42}$ pre-fibrillar structure: (E) initial structure; (F) initial separation of the units after 50 ns; (G) Rearrangement of the interaction between Asp23 and Lys28; (H) Dissociation of the units. After the dissociation at 60 ns, no spontaneous formation of the fibrillar structure was observed in a 300 ns-long MD simulation.

suggesting a chain polymerization potential (Fig. 6D). However, when the same structure was simulated with an AA molecule docked between the two units, we observed competition for the interaction with Asp23 and Lys28, resulting in new interactions between the two strands of each unit that stabilize them and prevent stacking (Fig. 6E–H). In this scenario, even after the spontaneous unbinding of the AA molecule, the $A\beta_{42}$ tetramer was not formed during a 300 ns simulation, indicating an AA-dependent effect on fibril formation (Figs. S3 and S4, Supporting Information). Taken together, the simulation data suggest a binding site for AA between the β-strands and that the interaction occurs with amino acid residues that are crucial for fibril formation. Once Lys28 and Asp23 are occupied by the interaction with AA, these 'charged clamps' undergo an intrastrand structural rearrangement, losing an important interaction for the stacking of adjacent strands.

## 4. Discussion

In conclusion, our study demonstrated the effective inhibition of $A\beta_{42}$ fibrillation by AA molecules. After 72 h of incubation, samples containing $A\beta_{42}$ co-incubated with AA presented 77% fewer orderly stacked β-sheet structures, which are characteristic of amyloid fibrils. In addition, while there is an increase in fluorescence intensity with time for samples with only $A\beta_{42}$, there is a decrease for $A\beta_{42}$ samples incubated with AA. These results suggest that AA can not only prevent aggregation but also disrupt preformed fibrillar aggregates. ITC experiments revealed the high affinity binding of AA molecules to $A\beta_{42}$, based on a positive cooperative binding model. Molecular docking and MD analyses revealed that AA molecules compete with other $A\beta_{42}$ monomers for binding to $A\beta_{42}$ oligomers at sites in the D23-K28 region. Studies have previously reported that during fibril formation, monomer strands are arranged to maximize hydrophobic interactions [40,46]. These conformational changes are stabilized by the salt bridge between D23 and K28 residues [46]. Therefore, our results suggest that AA prevents the formation of amyloid fibrils by binding to small $A\beta_{42}$ oligomers, which causes their disassembly. It is also reported that mutations in the D23-K28 region lead to early-onset AD [47,48]. For example, in the familial Iowa mutant, negatively charged aspartic acid (D23) is replaced by neutral asparagine resulting in decreased electrostatic repulsion of oligomers and increased aggregation rate [49,50]. Kai et al. also demonstrated that Tabersonine, a natural product from Voacanga Africana, disrupts the D23-K28 salt bridge and inhibits the formation of $A\beta_{42}$ fibrils [35]. Therefore, molecules that act in this region, such as AA, are promising to prevent the early development of the disease.

Based on these findings, supplementation or targeted delivery of AA to the brain may present a promising strategy to prevent neurodegeneration caused by amyloid plaques. As a potential candidate drug for AD therapy, AA is advantageous because it crosses the blood-brain barrier and accumulates close to neurons. We highlight that this inhibitor is a low-cost natural compound and that its therapeutic effect may be achieved at low concentrations, contributing to the development of an accessible therapy. The binding model between AA and $A\beta_{42}$ can be explored in the design of novel drugs for other amyloidogenic diseases.

## Author contributions

I.S: Conceptualization, Methodology, Data analyses, Writing – original draft, review and editing; F.Q.: Conceptualization, Methodology, Data analyses, Writing – review and editing; P.M.P.L.: Methodology, Data analyses, Writing – review and editing; A.S.N.: Methodology, Data analyses, Writing – review and editing; V.Z.: Writing - Review & Editing, Funding acquisition, Supervision.

## Declaration of competing interest

The authors declare that they have no known competing financial interests or personal relationships that could have appeared to influence the work reported in this paper.

## Acknowledgments

We gratefully acknowledge the National Council for Scientific and Technological Development - CNPq (Grant numbers 381473/2019-8 and 120639/2019-0) and Sao Paulo Research Foundation - FAPESP (Grant number 2017/21869-6) for their financial support. We also acknowledge the researchers from Nanomedicine and Nanotoxicology Group/IFSC/USP for their kind cooperation in this study.

## Appendix A. Supplementary data

Supplementary data to this article can be found online at https://doi.org/10.1016/j.biochi.2022.05.006.

## References

[1] D.S. Roy, A. Arons, T.I. Mitchell, M. Pignatelli, T.J. Ryan, S. Tonegawa, Memory retrieval by activating engram cells in mouse models of early Alzheimer's disease, Nature 531 (2016) 508–512, https://doi.org/10.1038/nature17172.
[2] T. Watanabe-Nakayama, K. Ono, M. Itami, R. Takahashi, D.B. Teplow, M. Yamada, High-speed atomic force microscopy reveals structural dynamics of amyloid β 1–42 aggregates, Proc. Natl. Acad. Sci. Unit. States Am. 113 (2016) 5835–5840, https://doi.org/10.1073/pnas.1524807113.
[3] J. Wang, B.J. Gu, C.L. Masters, Y.J. Wang, A systemic view of Alzheimer disease - insights from amyloid-β metabolism beyond the brain, Nat. Rev. Neurol. 13 (2017) 612–623, https://doi.org/10.1038/nrneurol.2017.111.
[4] F. Panza, M. Lozupone, G. Logroscino, B.P. Imbimbo, A critical appraisal of amyloid-β-targeting therapies for Alzheimer disease, Nat. Rev. Neurol. 15 (2019) 73–88, https://doi.org/10.1038/s41582-018-0116-6.
[5] Y. Xiao, B. Ma, D. McElheny, S. Parthasarathy, F. Long, M. Hoshi, R. Nussinov, Y. Ishii, Aβ(1-42) fibril structure illuminates self-recognition and replication of amyloid in Alzheimer's disease, Nat. Struct. Mol. Biol. 22 (2015) 499–505, https://doi.org/10.1038/nsmb.2991.
[6] M. Ahmed, J. Davis, D. Aucoin, T. Sato, S. Ahuja, S. Aimoto, J.I. Elliott, W.E. Van Nostrand, S.O. Smith, Structural conversion of neurotoxic amyloid-b 1-42 oligomers to fibrils, Nat. Struct. Mol. Biol. 17 (2010) 561–567, https://doi.org/10.1038/nsmb.1799.
[7] G.F. Chen, T.H. Xu, Y. Yan, Y.R. Zhou, Y. Jiang, K. Melcher, H.E. Xu, Amyloid beta: structure, biology and structure-based therapeutic development, Acta Pharmacol. Sin. 38 (2017) 1205–1235, https://doi.org/10.1038/aps.2017.28.
[8] M. Serra-Batiste, M. Ninot-Pedrosa, M. Bayoumi, M. Gairí, G. Maglia, N. Carulla, Aβ42 assembles into specific β-barrel pore-forming oligomers in membrane-mimicking environments, Proc. Natl. Acad. Sci. Unit. States Am. 113 (2016) 10866–10871, https://doi.org/10.1073/pnas.1605104113.
[9] X. Qian, B. Hamad, G. Dias-Lalcaca, The Alzheimer disease market, Nat. Rev. Drug Discov. 14 (2015) 675–676, https://doi.org/10.1038/nrd4749.
[10] G. Kashyap, D. Bapat, D. Das, R. Gowaikar, R.E. Amritkar, G. Rangarajan, V. Ravindranath, G. Ambika, Synapse loss and progress of Alzheimer's disease -A network model, Sci. Rep. 9 (2019) 1–9, https://doi.org/10.1038/s41598-019-43076-y.
[11] O. Prikhodko, K.D. Rynearson, T. Sekhon, M.M. Mante, S. Diego, H. System, L. Jolla, The GSM BPN-15606 as a potential candidate for preventative therapy in alzheimer ' s disease, J. Alzheim. Dis. 73 (2020) 1541–1554, https://doi.org/10.3233/JAD-190442.
[12] D.J. Selkoe, Alzheimer disease and aducanumab: adjusting our approach, Nat. Rev. Neurol. 15 (2019) 365–366, https://doi.org/10.1038/s41582-019-0205-1.
[13] L.-F. Yang, Cheng-Ming Zeng, The degradation products of ascorbic acid inhibit amyloid fibrillation of insulin and destabilize preformed fibrils, Molecules 23 (2018), https://doi.org/10.3390/molecules23123122.
[14] A.C. Carr, S. Maggini, Vitamin C and immune function, Nutrients 9 (2017), https://doi.org/10.3390/nu5072502.
[15] F. Monacelli, E. Acquarone, C. Giannotti, R. Borghi, A. Nencioni, Vitamin C, aging and Alzheimer's disease, Nutrients 9 (2017) 1–26, https://doi.org/10.3390/nu9070670.
[16] A. Covarrubias-Pinto, A.I. Acuña, F.A. Beltrán, L. Torres-Díaz, M.A. Castro, Old things new view: ascorbic acid protects the brain in neurodegenerative disorders, Int. J. Mol. Sci. 16 (2015) 28194–28217, https://doi.org/10.3390/ijms161226095.
[17] G.L. Bowman, H. Dodge, B. Frei, C. Calabrese, B.S. Oken, J.A. Kaye, J.F. Quinn, Ascorbic acid and rates of cognitive decline in Alzheimer's disease, J. Alzheim. Dis. 16 (2009) 93–98, https://doi.org/10.3233/JAD-2009-0923.

[18] P. Alam, A.Z. Beg, M.K. Siddiqi, S.K. Chaturvedi, R.K. Rajpoot, M.R. Ajmal, M. Zaman, A.S. Abdelhameed, R.H. Khan, Ascorbic acid inhibits human insulin aggregation and protects against amyloid induced cytotoxicity, Arch. Biochem. Biophys. 621 (2017) 54–62, https://doi.org/10.1016/j.abb.2017.04.005.
[19] S. Dixit, A. Bernardo, J.M. Walker, J.A. Kennard, G.Y. Kim, E.S. Kessler, F.E. Harrison, Vitamin C deficiency in the brain impairs cognition, increases amyloid accumulation and deposition, and oxidative stress in APP/PSEN1 and normally aging mice, ACS Chem. Neurosci. 6 (2015) 570–581, https://doi.org/10.1021/cn500308h.
[20] K. Hashimoto, T. Ishima, Y. Sato, D. Bruno, J. Nierenberg, C.R. Marmar, H. Zetterberg, K. Blennow, N. Pomara, Increased levels of ascorbic acid in the cerebrospinal fluid of cognitively intact elderly patients with major depression: a preliminary study, Sci. Rep. 7 (2017) 1–7, https://doi.org/10.1038/s41598-017-03836-0.
[21] J. Kocot, D. Luchowska-Kocot, M. Kiełczykowska, I. Musik, J. Kurzepa, Does vitamin c influence neurodegenerative diseases and psychiatric disorders? Nutrients 9 (2017) https://doi.org/10.3390/nu9070659.
[22] S.-Y. Kook, K.-M. Lee, Y. Kim, M.-Y. Cha, S. Kang, S.H. Baik, H. Lee, R. Park, I. Mook-Jung, High-dose of vitamin C supplementation reduces amyloid plaque burden and ameliorates pathological changes in the brain of 5XFAD mice, Cell Death Dis. 5 (2014), e1083, https://doi.org/10.1038/cddis.2014.26.
[23] M. Noguchi-Shinohara, C. Abe, S. Yuki-Nozaki, C. Dohmoto, A. Mori, K. Hayashi, S. Shibata, Y. Ikeda, K. Sakai, K. Iwasa, M. Yokogawa, M. Ishimiya, H. Nakamura, H. Yokoji, K. Komai, H. Nakamara, M. Yamada, Higher Blood Vitamin C Levels are Associated with Reduction of Apolipoprotein e E4-related Risks of Cognitive Decline in Women: the Nakajima Study, J. Alzheim. Dis. 63 (2018) 1289–1297, https://doi.org/10.3233/JAD-170971.
[24] P. Patel, K. Parmar, D. Patel, S. Kumar, M. Trivedi, M. Das, Inhibition of amyloid fibril formation of lysozyme by ascorbic acid and a probable mechanism of action, Int. J. Biol. Macromol. 114 (2018) 666–678, https://doi.org/10.1016/j.ijbiomac.2018.03.152.
[25] C. Ritter, M. Adrian, D. Riek-loher, B. Bohrmann, H. Do, D. Schubert, R. Riek, 3D structure of Alzheimer's amyloid-b (1-42) fibrils, Proc. Natl. Acad. Sci. U.S.A. 102 (2005) 17342–17347.
[26] H. Dos Santos Muniz, A.S. Nascimento, Ligand- and receptor-based docking with LiBELa, J. Comput. Aided Mol. Des. 29 (2015) 713–723, https://doi.org/10.1007/s10822-015-9856-1.
[27] D.A. Case, T.E. Cheatham, T. Darden, H. Gohlke, R. Luo, K.M. Merz, A. Onufriev, C. Simmerling, B. Wang, R.J. Woods, The Amber biomolecular simulation programs, J. Comput. Chem. 26 (2005) 1668–1688, https://doi.org/10.1002/jcc.20290.
[28] R. Salomon-Ferrer, D.A. Case, R.C. Walker, An overview of the Amber biomolecular simulation package, WIREs Comput. Mol. Sci. 3 (2013) 198–210, https://doi.org/10.1002/wcms.1121.
[29] S. Le Grand, A.W. Götz, R.C. Walker, SPFP: speed without compromise - a mixed precision model for GPU accelerated molecular dynamics simulations, Comput. Phys. Commun. 184 (2013) 374–380, https://doi.org/10.1016/j.cpc.2012.09.022.
[30] D.R. Roe, T.E. Cheatham, PTRAJ and CPPTRAJ: software for processing and analysis of molecular dynamics trajectory data, J. Chem. Theor. Comput. 9 (2013) 3084–3095, https://doi.org/10.1021/ct400341p.
[31] A.S. Nascimento, AmberEnergy++ (n.d.), https://github.com/alessandronascimento/amberenergy. (Accessed 3 May 2021).
[32] W. Humphrey, A. Dalke, K. Schulten, VMS: visual molecular dynamics, J. Mol. Graph. 14 (1996) 33–38.
[33] E.F. Pettersen, T.D. Goddard, C.C. Huang, G.S. Couch, D.M. Greenblatt, E.C. Meng, T.E. Ferrin, UCSF Chimera - a visualization system for exploratory research and analysis, J. Comput. Chem. 25 (2004) 1605–1612, https://doi.org/10.1002/jcc.20084.
[34] Q. Fan, Y. Liu, X. Wang, Z. Zhang, Y. Fu, L. Liu, P. Wang, H. Ma, H. Ma, N.P. Seeram, J. Zheng, F. Zhou, Ginnalin A inhibits aggregation, reverses fibrillogenesis, and alleviates cytotoxicity of amyloid β(1-42), ACS Chem. Neurosci. 11 (2020) 638–647, https://doi.org/10.1021/acschemneuro.9b00673.
[35] T. Kai, L. Zhang, X. Wang, A. Jing, B. Zhao, X. Yu, J. Zheng, F. Zhou, Tabersonine inhibits amyloid fibril formation and cytotoxicity of aβ(1-42), ACS Chem. Neurosci. 6 (2015) 879–888, https://doi.org/10.1021/acschemneuro.5b00015.
[36] M. Törnquist, R. Cukalevski, U. Weininger, G. Meisl, T.P.J. Knowles, T. Leiding, Ultrastructural evidence for self-replication of Alzheimer-associated A β 42 amyloid along the sides of fibrils, Proc. Natl. Acad. Sci. Unit. States Am. 117 (2020) 11265–11273, https://doi.org/10.1073/pnas.1918481117.
[37] M. Mold, L. Ouro-Gnao, B.M. Wieckowski, C. Exley, Copper prevents amyloid-β1-42from forming amyloid fibrils under near-physiological conditions in vitro, Sci. Rep. 3 (2013) 1–6, https://doi.org/10.1038/srep01256.
[38] K. Ezzat, M. Pernemalm, S. Pålsson, T.C. Roberts, P. Järver, A. Dondalska, B. Bestas, M.J. Sobkowiak, B. Levänen, M. Sköld, E.A. Thompson, O. Saher, O.K. Kari, T. Lajunen, E. Sverremark Ekström, C. Nilsson, Y. Ishchenko, T. Malm, M.J.A. Wood, U.F. Power, S. Masich, A. Lindén, J.K. Sandberg, J. Lehtiö, A.L. Spetz, S. EL Andaloussi, The viral protein corona directs viral pathogenesis and amyloid aggregation, Nat. Commun. 10 (2019) 1–16, https://doi.org/10.1038/s41467-019-10192-2.
[39] D. Jiang, I. Rauda, S. Han, S. Chen, F. Zhou, Aggregation pathways of the amyloid β(1 42) peptide depend on its colloidal stability and ordered β-sheet stacking, Langmuir 28 (2012) 12711–12721, https://doi.org/10.1021/la3021436.
[40] W. Hoyer, C. Grönwall, A. Jonsson, S. Ståhl, T. Härd, Stabilization of a β-hairpin in monomeric Alzheimer's amyloid-β peptide inhibits amyloid formation, Proc. Natl. Acad. Sci. Unit. States Am. 105 (2008) 5099–5104, https://doi.org/10.1073/pnas.0711731105.
[41] S. Slavkovic, Y. Zhu, Z.R. Churcher, A.A. Shoara, A.E. Johnson, P.E. Johnson, Thermodynamic analysis of cooperative ligand binding by the ATP-binding DNA aptamer indicates a population-shift binding mechanism, Sci. Rep. 10 (2020) 1–10, https://doi.org/10.1038/s41598-020-76002-8.
[42] N.S. Koulakiotis, P. Purhonen, E. Gikas, H. Hebert, A. Tsarbopoulos, Crocus-derived compounds alter the aggregation pathway of Alzheimer's Disease: associated beta amyloid protein, Sci. Rep. 10 (2020) 1–10, https://doi.org/10.1038/s41598-020-74770-x.
[43] T. Farkhondeh, S. Samarghandian, A.M. Pourbagher-Shahri, M. Sedaghat, The impact of curcumin and its modified formulations on Alzheimer's disease, J. Cell. Physiol. (2019) 16953–16965, https://doi.org/10.1002/jcp.28411.
[44] J. Lakey-Beitia, Y. González, D. Doens, D.E. Stephens, R. Santamaría, E. Murillo, M. Gutiérrez, P.L. Fernández, K.S. Rao, O.V. Larionov, A.A. Durant-Archibold, Assessment of novel curcumin derivatives as potent inhibitors of inflammation and amyloid-β aggregation in Alzheimer's disease, J. Alzheim. Dis. 60 (2017), https://doi.org/10.3233/JAD-170071. S59–S68.
[45] Y. Zheng, P. Wang, S. Li, X. Geng, L. Zou, M. Jin, Q. Zou, Q. Wang, X. Yang, K. Wang, Development of DNA aptamer as a β-amyloid aggregation inhibitor, ACS Appl. Bio Mater. 3 (12) (2020), https://doi.org/10.1021/acsabm.0c00996.
[46] G. Reddy, J.E. Straub, D. Thirumalai, Influence of preformed Asp23-Lys28 salt bridge on the conformational fluctuations of monomers and dimers of Aβ peptides with implications for rates of fibril formation, J. Phys. Chem. B 113 (2009) 1162–1172, https://doi.org/10.1021/jp808914c.
[47] B. Chandra, D. Bhowmik, B.K. Maity, K.R. Mote, D. Dhara, R. Venkatramani, S. Maiti, P.K. Madhu, Major reaction coordinates linking transient amyloid-β oligomers to fibrils measured at atomic level, Biophys. J. 113 (2017) 805–816, https://doi.org/10.1016/j.bpj.2017.06.068.
[48] N. Rezaei-Ghaleh, M. Amininasab, K. Giller, S. Kumar, A. Stündl, A. Schneider, S. Becker, J. Walter, M. Zweckstetter, Turn plasticity distinguishes different modes of amyloid-β aggregation, J. Am. Chem. Soc. 136 (2014) 4913–4919, https://doi.org/10.1021/ja411707y.
[49] P.M. Pifer, E.A. Yates, J. Legleiter, Point mutations in Aβ result in the formation of distinct polymorphic aggregates in the presence of lipid bilayers, PLoS One 6 (2011), https://doi.org/10.1371/journal.pone.0016248.
[50] S.T. Ngo, H.T. Thu Phung, K.B. Vu, V.V. Vu, Atomistic investigation of an Iowa Amyloid-β trimer in aqueous solution, RSC Adv. 8 (2018) 41705–41712, https://doi.org/10.1039/c8ra07615d.